Isomeric Excitation of ^{229}Th in Laser-Heated Clusters

Jintao Qi,* Hanxu Zhang,* and Xu Wang†
Graduate School, China Academy of Engineering Physics, Beijing 100193, China

(Received 10 August 2022; revised 1 October 2022; accepted 2 March 2023; published 16 March 2023)

We consider theoretically isomeric excitation of ^{229}Th in a laser-heated cluster. A ^{229}Th cluster is first radiated by an intense femtosecond laser pulse, causing ionization of the constituting atoms. The cluster will then survive for a time on the order of 1 ps, during which the electrons collide with the nuclei repeatedly and excite them to the isomeric state. Two mechanisms are responsible for the isomeric excitation: nuclear excitation by electron capture (NEEC) and nuclear excitation by inelastic electron scattering (NEIES). By changing the laser intensity, one can tune between NEEC and NEIES continuously. This laser-heated-cluster scheme not only provides a highly efficient means for isomeric excitation, but also provides an approach for the confirmation of the NEEC process, which has been predicted for over forty years without conclusive experimental verifications.

DOI: 10.1103/PhysRevLett.130.112501

Introduction.—The ^{229}Th nucleus has a low-lying isomeric state with energy around 8.28 eV above the ground state [1–5]. This isomeric state, denoted ^{229m}Th (half-life on the order of 10^{-6} s via internal conversion, 10^{3} s via γ decay, spin-parity $3/2^{+}$), has fascinated the scientific community for potential applications in nuclear optical clocks [6–9], nuclear lasers [10], checking variations of fundamental constants [11–13], etc. Additionally, it provides an intriguing platform on which nuclear physics, atomic physics, and laser physics directly interplay [14].

From decay reactions, ^{229m}Th can be obtained from α decay of ^{233}U [15,16] or β decay of ^{229}Ac [17]. The former suffers from low production yield due to the long decay half-life (1.6×10^{5} yr) and the low branching ratio (2%) to the isomeric state, as well as an 84-keV recoil energy. The latter suffers from low production yield of ^{229}Ac. Exploring for efficient *active* excitation methods is the focus of recent research, for example: (i) Direct optical excitation using vacuum ultraviolet light has been attempted by several groups without positive results [18–21]. (ii) Indirect optical excitation via the second excited state [22] using 29-keV synchrotron radiation has been demonstrated experimentally [23]. The excitation probability for a single ^{229}Th nucleus is on the order of 10^{-11} per second. (iii) Electronic-bridge processes have been proposed for various systems [24–28]. Experimental realization has not been reported, possibly due to high requirements on resonant conditions. (iv) Inelastic scattering of low-energy electrons [29,30] or muons [31] has been calculated to have relatively high-excitation cross sections. (v) In strong laser pulses, the ^{229}Th nucleus can be excited by a laser-driven electron recollision process [32,33]. The excitation probability for a single ^{229}Th nucleus is calculated to be on the order of 10^{-12} per femtosecond laser pulse [33].

In this Letter, we consider isomeric excitation of ^{229}Th in a laser-heated cluster (metal clusters, or nanoparticles, can be generated by physical, chemical, or biological approaches [34,35]). The idea is illustrated in Fig. 1. An intense femtosecond laser pulse radiates on a ^{229}Th cluster, causing ionization of the constituting atoms. After the laser pulse is over, most of the emitted electrons will be confined in the cluster, colliding with and exciting the ^{229}Th nuclei repeatedly. This collision and nuclear-excitation process lasts for a time on the order of 1 ps, the lifetime of the cluster after laser radiation. Isomeric excitation happens dominantly via two mechanisms: nuclear excitation by electron capture (NEEC) and nuclear excitation by inelastic electron scattering (NEIES). In NEEC (NEIES) the nucleus is excited by the energy released from free-bound (free-free)

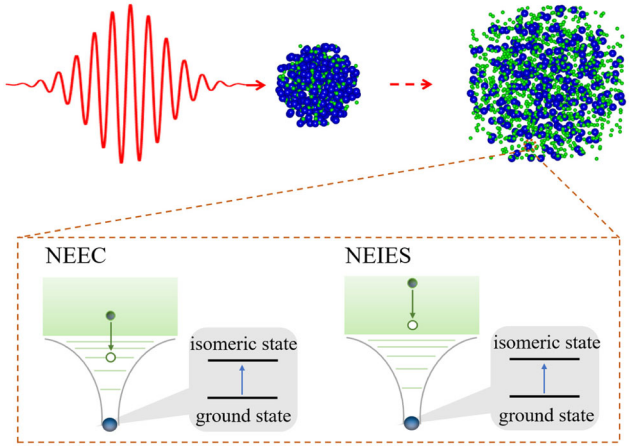

FIG. 1. Schematic illustration of ^{229}Th isomeric excitation in a laser-heated cluster. After being radiated by an intense femtosecond laser pulse, the cluster survives for a time on the order of 1 ps, during which isomeric excitation happens via NEEC and NEIES.

electronic transitions. Other mechanisms, including nuclear excitation by bound-bound electronic transitions and photoexcitations, are at least several orders of magnitude weaker (estimations are given in the Supplemental Material [36]).

This laser-heated-cluster scheme provides a nanoplasma environment of solid-state density during the lifetime of the cluster [51–60], leading to highly efficient isomeric excitation: calculations show that a ^{229m}Th is generated from every 10^6–10^7 nuclei. In addition to the high-excitation efficiency, and perhaps more interestingly from the physical point of view, this scheme provides a convenient means for controlling nuclear-excitation mechanisms. We find that, with relatively low laser intensities ($\approx 10^{14}$ W/cm^2), the excitation mechanism is dominantly NEEC, whereas with relatively high laser intensities ($\approx 10^{16}$ W/cm^2), the excitation mechanism is dominantly NEIES. One can tune between these two mechanisms continuously by simply changing the laser intensity. A particularly intriguing possibility is that this scheme provides an alternative approach for the confirmation of the NEEC process [61–63]. Currently two beam-based experiments aim to confirm NEEC with ^{93m}Mo, but contradicting results are reported. Chiara *et al.* observe an isomer depletion and attribute it to NEEC [64], but the results cannot be explained by theoretical calculations [65–67]. Guo *et al.* perform a similar experiment, but signature of isomer depletion is not observed [68].

Laser-cluster interaction and cluster expansion.—In the current study, the ^{229}Th cluster is assumed to have 10^6 atoms. Using the atomic density $n_0 = 3.03 \times 10^{28}$ m^{-3}, the cluster radius is 19.8 nm. Two initial cluster setups have been tried. In the first one, the cluster is composed of neutral atoms without free electrons. In the second one, the cluster is composed of first-charged ions and 10^6 free electrons, which occupy energy levels up to the Fermi energy. The second setup seems to be closer to our picture of a metal cluster. However, we find that these two setups lead to almost identical particle densities and electron energy distributions after the laser pulse is over and during cluster expansion, hence to nearly identical nuclear-excitation yields. Therefore, in the following, we only show results from the first setup.

The interaction of the cluster with the laser pulse and subsequent expansion of the cluster are calculated using standard 2D three-velocity particle-in-cell (PIC) simulations with the EPOCH code [69]. The simulation box size is 1×1 μm and the mesh size is 1×1 nm. The laser pulse is linearly polarized with wavelength 800 nm and a Gaussian temporal envelope of duration 30 fs (full width at half maximum for intensity).

The laser pulse ionizes the atoms and free electrons are generated. Most of these electrons will, however, be confined in the cluster. This is related to the condition that the laser intensities used here are relatively low, so the electron energies are mostly on the order of 1–10 eV, which are most efficient in isomeric excitation of ^{229}Th. This is in contrast to most other studies on laser-cluster interaction, which usually use much higher intensities [51–60]. For a laser pulse with peak intensity 10^{15} W/cm^2, roughly four electrons are emitted from each atom, in line with estimations from the Ammosov-Delone-Krainov tunnel-ionization formula [70]. The electron density is then about 4 times higher than the ion density after the pulse is over, as shown in Fig. 2(a). We have checked that the probability of electron impact ionization [71] is smaller by about 4 orders of magnitude, so almost all ionizations come from field ionization.

After being radiated by the laser pulse, the cluster starts to expand due to hydrodynamic forces from the confined electrons and Coulomb repulsions between the ions. The timescale of cluster expansion is usually on the order of 1 ps. During this time, the electrons and the ions maintain high densities. Figure 2(b) shows the radius-resolved density distributions of the ions and of the electrons at three time steps, namely, 0.1, 1, and 2 ps. Particles near the surface of the cluster expand first, followed by insider

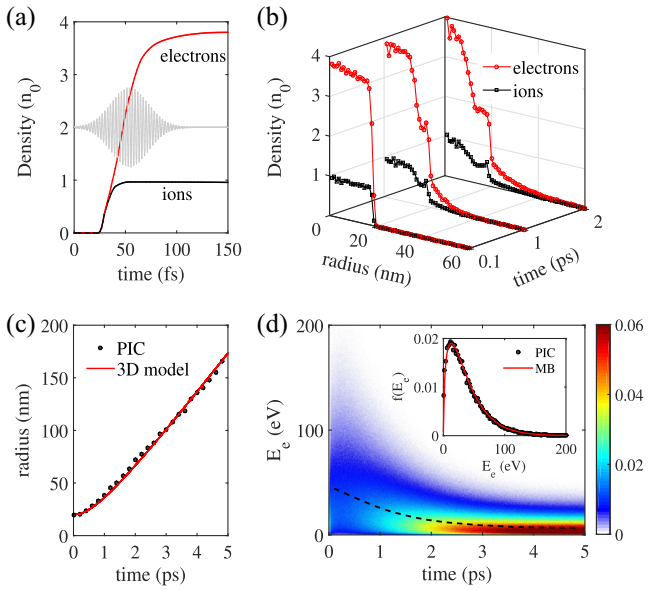

FIG. 2. (a) Average densities of ^{229}Th ions and of the electrons in the cluster during a laser pulse of peak intensity 10^{15} W/cm^2. $n_0 = 3.03 \times 10^{28}$ m^{-3} is the original density of the ^{229}Th atoms. The duration of the laser pulse is shown as the gray background. (b) Radius-resolved densities of ^{229}Th ions and of the electrons during cluster expansion at 0.1, 1, and 2 ps. (c) Temporal evolution of the cluster radius, from the PIC simulation and from a 3D cluster expansion model. (d) Temporal evolution of the electron kinetic energy distribution in the cluster. The color bar denotes the value of the distribution function $f(E_e)$. The inset shows the comparison of the electron kinetic energy distribution at 1 ps and a Maxwell-Boltzmann (MB) distribution with temperature 26 eV. The black dashed curve in the main figure marks the evolution of the electron temperature.

particles. The interesting characteristic of cluster expansion is that even if the outermost layer of the cluster has expanded relatively far, the high-density core can still exist, which is similar to the original cluster size. This can be seen, for example, from the density distributions at 1 and 2 ps. The evolution of cluster radius is shown in Fig. 2(c). Here the radius of the cluster at each time is obtained by averaging the positions of the outmost 500 ions. The PIC simulation results agree well with a three-dimensional (3D) cluster expansion model [55], taking into account the hydrodynamic forces from the confined electrons and the Coulomb repulsions between the ions. It is to be emphasized that, although the outermost layer of the cluster expands to a relatively large radius, it is the high-density core that makes the major contribution to nuclear excitation.

The temporal evolution of the electron kinetic energy distribution in the cluster is shown in Fig. 2(d). Inside the cluster, this distribution is position independent. During the laser pulse (< 0.1 ps), the electrons are emitted from the atoms and accelerated by the laser field. The average energy of the electrons is on the order of the ponderomotive energy U_p, which equals 59.8 eV for 10^{15} W/cm^2 and 800 nm. Then the electrons collide repeatedly with the ions and with other electrons, and the kinetic energy distribution soon approaches a thermal distribution. For example, the inset of Fig. 2(d) shows the kinetic energy distribution at 1 ps in comparison to a Maxwell-Boltzmann distribution with temperature 26 eV. As the cluster expands, the electron temperature decreases to a few electronvolts (8.8 eV at 3 ps, 7.3 eV at 4 ps, and 6.8 eV at 5 ps), as marked by the black dashed curve.

Nuclear isomeric excitation.—Cluster-confined high-density electrons excite the ^{229}Th nuclei via NEEC and NEIES. The mechanism is NEEC (NEIES) if the electron kinetic energy is lower (higher) than the isomeric energy of 8.28 eV. Figure 3 shows the isomeric-excitation cross section for ^{229}Th^{1+}. The discrete δ-function-like vertical lines for $E_e < 8.28$ eV are due to the resonant feature of NEEC. The vertical lines become denser as E_e approaches 8.28 eV due to capture to highly excited states. Note that the vertical lines actually have very small widths and finite heights (exceeding the vertical range of the main figure, though) due to finite lifetime of the isomeric state and the atomic excited states, as shown, for example, by the inset. The width of the leftmost vertical line is about 8×10^{-11} eV. For $E_e > 8.28$ eV, the mechanism is NEIES and the cross section is continuous.

The cross sections in Fig. 3 are calculated with a Dirac distorted wave Born approximation, and the detailed theoretical framework can be found in Ref. [30] (a brief outline is given in the Supplemental Material [36], Sec. 1). For other ionic states, the cross sections for NEEC will change according to the energies of the involved bound states (shown in the Supplemental Material [36], Sec. 2),

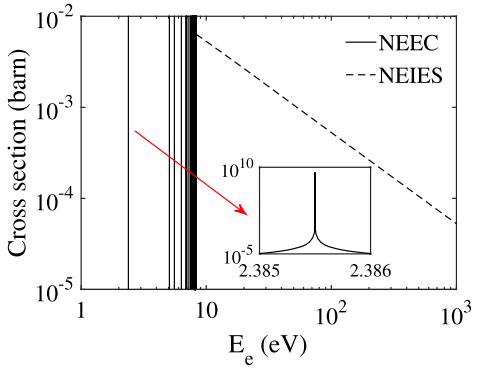

FIG. 3. Total $(E2 + M1)$ isomeric-excitation cross section for ^{229}Th^{1+}. For $E_e < 8.28$ eV, the mechanism is NEEC; for $E_e > 8.28$ eV, the mechanism is NEIES. The NEEC "vertical lines" have heights exceeding the vertical range of the main figure. The leftmost vertical line in full range is shown by the inset.

whereas the cross sections for NEIES are almost identical to the Th^{1+} case [29,30]. The electron wave functions are calculated using the code RADIAL [72]. In calculating NEEC, we have assumed the ions to be in their ground states, although Gargiulo *et al.* recently predicted that the cross sections can be enhanced for excited ions [73]. In obtaining Fig. 3, we have used reduced nuclear transition probabilities $B(E2) = 27$ and $B(M1) = 0.0076$ W.u. [74]. Here $E2$ or $M1$ means electric quadrupole or magnetic dipole transitions, respectively. Electric dipole transition is forbidden due to parity. Benchmarks of our calculations against available results in the literature are given in the Supplemental Material [36], Sec. 3.

The rate of exciting a single ^{229}Th nucleus located at distance r from the cluster center is

$$\Gamma(r,t) = n_e(r,t) \int dE_e f(E_e,t) v_e(E_e) \times \sum_q P_q [\sigma^q_{\mathrm{NEEC}}(E_e) + \sigma^q_{\mathrm{NEIES}}(E_e)], \quad (1)$$

where $n_e(r,t)$ is the density of the electrons, $f(E_e,t)$ is the normalized distribution function of the electron kinetic energy, and $v_e(E_e) = \sqrt{2E_e}$ is the electron velocity. P_q is the probability in the qth ionic state, and $\sigma^q_{\mathrm{NEEC\text{-}NEIES}}(E_e)$ is the corresponding NEEC-NEIES cross section. The ion charge distribution P_q depends on the laser intensity, as discussed in the Supplemental Material [36], Sec. 5. If the integration is performed for $E_e < 8.28$ eV, one gets the excitation rate for NEEC. Otherwise, one gets the excitation rate for NEIES. The production yield of ^{229m}Th is obtained by integrations over time and the cluster volume,

$$Y_{\mathrm{exc}}(t) = 4\pi \int_0^t dt' \int_0^\infty n_i(r,t') \Gamma(r,t') r^2 dr, \quad (2)$$

where $n_i(r,t)$ is the time-dependent ion density.

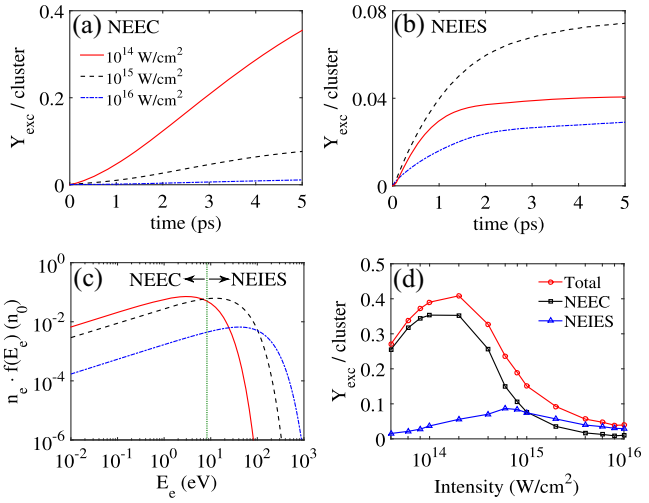

FIG. 4. (a) Production yield of ^{229m}Th per cluster from NEEC under three laser intensities. (b) Production yield of ^{229m}Th per cluster from NEIES under the same three laser intensities. (c) Electron kinetic energy distributions in the cluster at time 1 ps during cluster expansion, for the same three laser intensities. (d) Production yield of ^{229m}Th per cluster as a function of laser peak intensity at 5 ps.

Figures 4(a) and 4(b) show the production yield $Y_{\mathrm{exc}}(t)$ per cluster for NEEC and NEIES, respectively, under three laser peak intensities, namely, 10^{14}, 10^{15}, and 10^{16} W/cm^2. One sees that the production yields keep increasing with time for several picoseconds. Even at 5 ps, tendencies of continuing (albeit slower) increase can be seen, especially for NEEC. One can find that, for NEEC, 10^{14} W/cm^2 is more efficient than the other two intensities, yielding about 0.35 per cluster at 5 ps. For NEIES, 10^{15} W/cm^2 is more efficient than the other two intensities, yielding about 0.08 per cluster at 5 ps.

These results can be understood by looking at the electron kinetic energy distributions corresponding to these three intensities, as displayed in Fig. 4(c). The energy distributions are obtained at time 1 ps. One can see that 10^{14} W/cm^2 produces more electrons in the NEEC regime, explaining the results in Fig. 4(a); 10^{15} W/cm^2 produces more electrons in the NEIES regime, especially those with relatively high NEIES cross sections (from Fig. 3, the energy region just above the 8.28 eV threshold corresponding to relatively high NEIES cross sections), explaining the results in Fig. 4(b).

In Fig. 4(d), we show the (total and separated) production yield per cluster as a function of laser peak intensity, at time 5 ps. One sees that the total yield peaks at 2×10^{14} W/cm^2 with a value of over 0.4 per cluster. The NEEC mechanism dominates with relatively low intensities, whereas the NEIES mechanism dominates with relatively high intensities. The two are nearly equal at 10^{15} W/cm^2. Laser intensity is therefore a very efficient knob to control the excitation mechanism. One can tune between NEEC and NEIES continuously by simply changing the laser intensity.

Discussion.—(a) Assume that we have 1 mg (10^{-3} g) of ^{229}Th prepared in the cluster form. The number of atoms is 2.6×10^{18} and the number of clusters is 2.6×10^{12}. After laser-cluster interaction, the number of ^{229m}Th generated is about $2.6 \times 10^{12} \times 0.4 \approx 1.0 \times 10^{12}$ with the optimal intensity of 2×10^{14} W/cm^2.

(b) We envisage an experimental scenario to confirm NEEC: (i) Radiate ^{229}Th clusters with laser intensity about 10^{14} W/cm^2, under which NEIES is much weaker than NEEC. Suppose the number of clusters in the laser focus is N, then the generated ^{229m}Th is about $0.3N$ [Fig. 4(d)]. (ii) Guide the ions after cluster expansion to a neutralization and detection system, such as the one used in [5]. From Sec. 5 of the Supplemental Material [36], the ions are roughly 70% Th^{2+} and 30% Th^{3+} under this intensity. The ions are neutralized, then the internal-conversion electrons can be detected by a multichannel plate detector. In [5] the ^{229}Th ions are generated from α decay of ^{233}U and guided to arrive in bunches, each bunch having about 400 ^{229}Th ions, among which about eight are ^{229m}Th (the 2% branching ratio). This is shown to lead to a signal-to-background ratio of about 300. In our case, each laser pulse generates an ion bunch after cluster expansion. If we want to achieve the same number of ^{229m}Th in each bunch, the number of clusters in the laser focus should be $N \approx 8/0.3 \approx 27$. In laser-cluster experiments, N is on the order of 10^3 [53,75,76], so even higher signal-to-background ratios can be expected. (iii) The above steps can be repeated for each laser pulse. The repetition rate can be adjusted according to the time needed in the detection step.

(c) Although laser-heated clusters are nanometer-size plasmas, they have key differences compared to plasma plumes generated from laser ablation on solid targets [77–81] (among which [81] is for ^{229}Th): (i) Cluster nanoplasmas have much simpler characteristics and dynamics than laser-ablated plasma plumes [82–84]. (ii) Cluster nanoplasmas have much higher densities, which emphasize NEEC and NEIES over competing mechanisms. To further isolate NEEC, one only needs to use laser intensities that favor NEEC over NEIES, as discussed above.

(d) We emphasize the important role of the laser intensity. A higher intensity leads to (i) a higher degree of ionization for each atom, (ii) higher electron kinetic energies, and (iii) faster cluster expansion due to stronger hydrodynamic and Coulomb repulsive forces. In the current study, the electron energies are on the order of 1–10 eV. For intensities of 10^{18}–10^{19} W/cm^2, the electron energies can be on the order of 1 MeV and excitations of higher nuclear states are possible.

Conclusion.—In this Letter, we consider isomeric excitation of ^{229}Th using laser-cluster interaction. An intense femtosecond laser pulse radiates on a ^{229}Th cluster and

ionizes the constituting atoms. The resulting high-density electrons will mostly be confined within the cluster, colliding with and exciting the nuclei repeatedly for a time on the order of 1 ps. We show that this scheme is very efficient in nuclear isomeric excitation, generating a ^{229m}Th nucleus from every 10^6–10^7 atoms. Besides the excitation efficiency, this scheme provides a method to tune between two major nuclear-excitation mechanisms, namely NEEC and NEIES, by simply changing the laser intensity. A particularly intriguing application of the proposed scheme is the potential confirmation of the NEEC process, which has been predicted theoretically for over forty years without a conclusive experimental confirmation.

We acknowledge funding support from NSFC No. 12088101 and No. 12147161.

*J. Q. and H. Z. contributed equally to this work.
†Corresponding author.
xwang@gscaep.ac.cn

[1] L. A. Kroger and C. W. Reich, Nucl. Phys. **A259**, 29 (1976).
[2] C. W. Reich and R. G. Helmer, Phys. Rev. Lett. **64**, 271 (1990).
[3] R. G. Helmer and C. W. Reich, Phys. Rev. C **49**, 1845 (1994).
[4] B. R. Beck, J. A. Becker, P. Beiersdorfer, G. V. Brown, K. J. Moody, J. B. Wilhelmy, F. S. Porter, C. A. Kilbourne, and R. L. Kelley, Phys. Rev. Lett. **98**, 142501 (2007).
[5] B. Seiferle *et al.*, Nature (London) **573**, 243 (2019).
[6] E. Peik and Chr. Tamm, Europhys. Lett. **61**, 181 (2003).
[7] W. G. Rellergert, D. DeMille, R. R. Greco, M. P. Hehlen, J. R. Torgerson, and E. R. Hudson, Phys. Rev. Lett. **104**, 200802 (2010).
[8] C. J. Campbell, A. G. Radnaev, A. Kuzmich, V. A. Dzuba, V. V. Flambaum, and A. Derevianko, Phys. Rev. Lett. **108**, 120802 (2012).
[9] K. Beeks, T. Sikorsky, T. Schumm, J. Thielking, M. V. Okhapkin, and E. Peik, Nat. Rev. Phys. **3**, 238 (2021).
[10] E. V. Tkalya, Phys. Rev. Lett. **106**, 162501 (2011).
[11] V. V. Flambaum, Phys. Rev. Lett. **97**, 092502 (2006).
[12] J. C. Berengut, V. A. Dzuba, V. V. Flambaum, and S. G. Porsev, Phys. Rev. Lett. **102**, 210801 (2009).
[13] P. Fadeev, J. C. Berengut, and V. V. Flambaum, Phys. Rev. A **102**, 052833 (2020).
[14] W. Wang, H. Zhang, and X. Wang, J. Phys. B **54**, 244001 (2021).
[15] V. Barci, G. Ardisson, G. Barci-Funel, B. Weiss, O. El Samad, and R. K. Sheline, Phys. Rev. C **68**, 034329 (2003).
[16] J. Thielking, M. V. Okhapkin, P. Głowacki, D. M. Meier, L. Wense, B. Seiferle, C. E. Düllmann, P. G. Thirolf, and E. Peik, Nature (London) **556**, 321 (2018).
[17] M. Verlinde, S. Kraemer, J. Moens, K. Chrysalidis, J. G. Correia *et al.*, Phys. Rev. C **100**, 024315 (2019).
[18] J. Jeet, C. Schneider, S. T. Sullivan, W. G. Rellergert, S. Mirzadeh, A. Cassanho, H. P. Jenssen, E. V. Tkalya, and E. R. Hudson, Phys. Rev. Lett. **114**, 253001 (2015).
[19] A. Yamaguchi, M. Kolbe, H. Kaser, T. Reichel, A. Gottwald, and E. Peik, New J. Phys. **17**, 053053 (2015).
[20] E. Peik and M. Okhapkin, C.R. Phys. **16**, 516 (2015).
[21] S. Stellmer, G. Kazakov, M. Schreitl, H. Kaser, M. Kolbe, and T. Schumm, Phys. Rev. A **97**, 062506 (2018).
[22] E. V. Tkalya, A. N. Zherikhin, and V. I. Zhudov, Phys. Rev. C **61**, 064308 (2000).
[23] T. Masuda *et al.*, Nature (London) **573**, 238 (2019).
[24] E. V. Tkalya, JETP Lett. **55**, 212 (1992).
[25] S. G. Porsev, V. V. Flambaum, E. Peik, and Chr. Tamm, Phys. Rev. Lett. **105**, 182501 (2010).
[26] P. V. Borisyuk, N. N. Kolachevsky, A. V. Taichenachev, E. V. Tkalya, I. Yu. Tolstikhina, and V. I. Yudin, Phys. Rev. C **100**, 044306 (2019).
[27] P. V. Bilous, H. Bekker, J. C. Berengut, B. Seiferle, L. vonderWense, P. G. Thirolf, T. Pfeifer, Jose R. Crespo Lopez-Urrutia, and A. Palffy, Phys. Rev. Lett. **124**, 192502 (2020).
[28] B. S. Nickerson, M. Pimon, P. V. Bilous, J. Gugler, K. Beeks, T. Sikorsky, P. Mohn, T. Schumm, and A. Pálffy, Phys. Rev. Lett. **125**, 032501 (2020).
[29] E. V. Tkalya, Phys. Rev. Lett. **124**, 242501 (2020).
[30] H. Zhang, W. Wang, and X. Wang, Phys. Rev. C **106**, 044604 (2022).
[31] E. V. Tkalya, Chin. Phys. C **45**, 094102 (2021).
[32] W. Wang, J. Zhou, B. Liu, and X. Wang, Phys. Rev. Lett. **127**, 052501 (2021).
[33] X. Wang, Phys. Rev. C **106**, 024606 (2022).
[34] R. Nagarajan, in *Nanoparticles: Synthesis, Stabilization, Passivation, and Functionalization* (American Chemical Society, Washington, DC, 2008), pp. 2–14.
[35] A. J. Shnoudeh, I. Hamad, R. W. Abdo, L. Qadumii, A. Y. Jaber, H. S. Surchi, and S. Z. Alkelany, in *Biomaterials and Bionanotechnology*, edited by R. K. Tekade (Academic Press, New York, 2019), pp. 527–612.
[36] See Supplemental Material at http://link.aps.org/supplemental/10.1103/PhysRevLett.130.112501 for calculation details and benchmarks, which includes Refs. [37–50].
[37] K. Alder, A. Bohr, T. Huus, B. Mottelson, and A. Winther, Rev. Mod. Phys. **28**, 432 (1956).
[38] V. B. Berestetskii, E. M. Lifshitz, and L. P. Pitaevskii, *Quantum Electrodynamics* (Butterworth-Heinemann, Oxford, UK, 1982), Vol. 4.
[39] E. V. Tkalya, Nucl. Phys. **A539**, 209 (1992).
[40] A. Bohr and B. R. Mottelson, *Nuclear Structure. Vol. I: Single-Particle Motion* (World Scientific, London, 1998).
[41] M. Abramowitz, I. A. Stegun, and R. H. Romer, *Handbook of Mathematical Functions with Formulas, Graphs, and Mathematical Tables* (National Bureau of Standards, Washington, D.C., 1964).
[42] B. Seiferle, L. von der Wense, and P. G. Thirolf, Phys. Rev. Lett. **118**, 042501 (2017).
[43] N. Minkov and A. Pálffy, Phys. Rev. C **103**, 014313 (2021).
[44] E. V. Tkalya, Phys. Rev. C **100**, 054316 (2019).
[45] A. Pálffy, Doctoral thesis, Justus-Liebig-University Giessen, 2006.
[46] A. Pálffy, J. Evers, and C. H. Keitel, Phys. Rev. C **77**, 044602 (2008).
[47] P. Ring and P. Schuck, *The Nuclear Many-Body Problem* (Springer, New York, 1980).
[48] H. W. Koch and J. Motz, Rev. Mod. Phys. **31**, 920 (1959).

[49] H. R. Griem, *Principles of Plasma Spectroscopy* (Cambridge University Press, Cambridge, 1997).
[50] R. P. Drake, *High-Energy-Density Physics* (Springer, Berlin, 2010).
[51] T. Ditmire, T. Donnelly, A. M. Rubenchik, R. W. Falcone, and M. D. Perry, Phys. Rev. A **53**, 3379 (1996).
[52] T. Ditmire, J. W. G. Tisch, E. Springate, M. B. Mason, N. Hay, R. A. Smith, J. Marangos, and M. H. R. Hutchinson, Nature (London) **386**, 54 (1997).
[53] T. Ditmire, J. Zweiback, V. P. Yanovsky, T. E. Cowan, G. Hays, and K. B. Wharton, Nature (London) **398**, 489 (1999).
[54] H. Wabnitz *et al.*, Nature (London) **420**, 482 (2002).
[55] V. P. Krainov and M. B. Smirnov, Phys. Rep. **370**, 237 (2002).
[56] F. Dorchies, F. Blasco, C. Bonte, T. Caillaud, C. Fourment, and O. Peyrusse, Phys. Rev. Lett. **100**, 205002 (2008).
[57] R. Rajeev, T. Madhu Trivikram, K. P. M. Rishad, V. Narayanan, E. Krishnakumar, and M. Krishnamurthy, Nat. Phys. **9**, 185 (2013).
[58] H. Park, Z. Wang, H. Xiong, S. B. Schoun, J. Xu, P. Agostini, and L. F. DiMauro, Phys. Rev. Lett. **113**, 263401 (2014).
[59] Z. Wang, A. Camacho Garibay, H. Park, U. Saalmann, P. Agostini, J. M. Rost, and L. F. DiMauro, Phys. Rev. Lett. **124**, 173201 (2020).
[60] J. Feng *et al.*, Phys. Rev. Lett. **128**, 052501 (2022).
[61] V. I. Goldanskii and V. A. Namiot, Phys. Lett. **62B**, 393 (1976).
[62] A. Pálffy, W. Scheid, and Z. Harman, Phys. Rev. A **73**, 012715 (2006).
[63] S. A. Karamian and J. J. Carroll, Phys. At. Nucl. **75**, 11 (2012).
[64] C. J. Chiara *et al.*, Nature (London) **554**, 216 (2018).
[65] Y. Wu, C. H. Keitel, and A. Pálffy, Phys. Rev. Lett. **122**, 212501 (2019).
[66] J. Rzadkiewicz, M. Polasik, K. Slabkowska, L. Syrocki, J. J. Carroll, and C. J. Chiara, Phys. Rev. Lett. **127**, 042501 (2021).
[67] S. Guo, Y. Fang, X. Zhou, and C. M. Petrache, Nature (London) **594**, E1 (2021).
[68] S. Guo, B. Ding, X. H. Zhou, Y. B. Wu, J. G. Wang *et al.*, Phys. Rev. Lett. **128**, 242502 (2022).
[69] T. D. Arber, K. Bennett, C. S. Brady, A. Lawrence-Douglas, M. G. Ramsay, N. J. Sircombe, P. Gillies, R. G. Evans, H. Schmitz, A. R. Bell, and C. P. Ridgers, Plasma Phys. Controlled Fusion **57**, 113001 (2015).
[70] M. V. Ammosov, N. B. Delone, and V. P. Krainov, Zh. Eksp. Teor. Fiz. **91**, 2008 (1986) [Sov. Phys. JETP **64**, 1191 (1986)].
[71] W. Lotz, Z. Phys. **232**, 101 (1970).
[72] F. Salvat and J. M. Fernández-Varea, Comput. Phys. Commun. **240**, 165 (2019).
[73] S. Gargiulo, I. Madan, and F. Carbone, Phys. Rev. Lett. **128**, 212502 (2022).
[74] N. Minkov and A. Pálffy, Phys. Rev. Lett. **118**, 212501 (2017).
[75] J. Zweiback, T. Ditmire, and M. D. Perry, Phys. Rev. A **59**, R3166 (1999).
[76] T. Ditmire, J. Zweiback, V. P. Yanovsky, T. E. Cowan, G. Hays, and K. B. Wharton, Phys. Plasmas **7**, 1993 (2000).
[77] M. R. Harston and J. F. Chemin, Phys. Rev. C **59**, 2462 (1999).
[78] G. Gosselin and P. Morel, Phys. Rev. C **70**, 064603 (2004).
[79] Y. Wu, J. Gunst, C. H. Keitel, and A. Pálffy, Phys. Rev. Lett. **120**, 052504 (2018).
[80] J. Gunst, Y. Wu, C. H. Keitel, and A. Pálffy, Phys. Rev. E **97**, 063205 (2018).
[81] P. V. Borisyuk, E. V. Chubunova, N. N. Kolachevsky, Yu. Yu. Lebedinskii, O. S. Vasiliev, and E. V. Tkalya, arXiv: 1804.00299.
[82] S. Amoruso, R. Bruzzese, N. Spinelli, and R. Velotta, J. Phys. B **32**, R131 (1999).
[83] J. König, S. Nolte, and A. Tünnermann, Opt. Express **13**, 10597 (2005).
[84] P. J. Skrodzki, M. Burger, I. Jovanovic, M. C. Phillips, J. Yeak, B. E. Brumfield, and S. S. Harilal, Phys. Plasmas **26**, 083508 (2019).